International Journal of Pharmaceutics 423 (2012) 489–495

Contents lists available at SciVerse ScienceDirect

International Journal of Pharmaceutics

journal homepage: www.elsevier.com/locate/ijpharm

Pharmaceutical nanotechnology

Boron nitride nanotubes radiolabeled with ^{99m}Tc: Preparation, physicochemical characterization, biodistribution study, and scintigraphic imaging in Swiss mice

Daniel Crístian Ferreira Soares[a,*], Tiago Hilário Ferreira[a], Carolina de Aguiar Ferreira[a], Valbert Nascimento Cardoso[b], Edésia Martins Barros de Sousa[a]

[a] Centro de Desenvolvimento da Tecnologia Nuclear (CDTN) – Laboratório de Materiais Nanoestruturados para Bioaplicações. Av. Antônio Carlos 6.627, Pampulha – 31270-901 Belo Horizonte, MG, Brazil
[b] Universidade Federal de Minas Gerais – Faculdade de Farmácia. Avenida Presidente Antônio Carlos, 6627 – Pampulha – 31270-901, Belo Horizonte, MG, Brazil

ARTICLE INFO

Article history:
Received 19 August 2011
Received in revised form
19 November 2011
Accepted 1 December 2011
Available online 9 December 2011

Keywords:
Functionalized boron nitride nanotubes
Physicochemical characterization
Biodistribution study and scintigraphic image

ABSTRACT

In the present study, boron nitride nanotubes (BNNTs) were synthesized from an innovative process and functionalized with a glycol chitosan polymer in CDTN (Centro de Desenvolvimento da Tecnologia Nuclear) laboratories. As a means of studying their *in vivo* biodistribution behavior, these nanotubes were radiolabeled with ^{99m}Tc and injected in mice. Their size, distribution, and homogeneity were determined by photon correlation spectroscopy (PCS), while their zeta potential was determined by laser Doppler anemometry. The morphology and structural organization were evaluated by scanning electron microscopy (SEM). The functionalization in the nanotubes was evaluated by thermogravimetry analysis (TGA) and Fourier transformer infrared spectroscopy. The results showed that BNNTs were obtained and functionalized successfully, reaching a mean size and dispersity deemed adequate for *in vivo* studies. The BNNTs were also evaluated by *ex vivo* biodistribution studies and scintigraphic imaging in healthy mice. The results showed that nanostructures, after 24 h, having accumulated in the liver, spleen and gut, and eliminated via renal excretion. The findings from this study reveal a potential application of functionalized BNNTs as new potential drugs or radioisotope nanocarriers to be applied in therapeutic procedures.

1. Introduction

The use of nanotechnology in the therapy of many diseases has been the target of many research activities, development, and innovation throughout industrialized countries worldwide (Huynh et al., 2009; Sakamoto et al., 2010). Nanostructured systems based on carbon, silica, gold, and metal oxides that integrate different forms, such as nanotubes, nanorods, nanowires, nanocages, nanoshells, and nanodisks, have been studied and applied to biological systems, especially from the functionalization (coating) with organic molecules, peptides, DNA fragments, antibodies, or hydrophilic polymers (Hocine et al., 2010; Klumpp et al., 2006). In this context, the functionalization process plays an important role in these nanostructures, improving the dispersibility in an aqueous medium and changing the *in vivo* biodistribution profile (Guo et al., 2007; Xiong et al., 2009). Several works published in recent decades have shown that the functionalization, or coating process, in different nanostructures using high hydrophilic molecules, like polyethylene glycol (PEG), can significantly increase their circulation time in the blood stream, in turn minimizing the aggregation of serum proteins, consequently reducing their identification by cells from the mononuclear phagocyte system (Safi et al., 2011; Vauthier et al., 2011). More recent studies have shown that the functionalization of nanostructures with specific molecules, such as folic acid or peptides (bombesin, for example), allows for these nanostructures to be more selectively accumulated in tumor cells, as compared to other non-target tissues. As such, these systems can be considered promising new carriers of drugs or radioisotopes with a high-specificity of action (de Barros et al., 2010; Soares et al., 2011).

Although this new approach appears to be the most effective means through which to improve the selectivity of nanostructured carriers for tumors, the passive tumor accumulation, using the EPR (enhanced permeability and retention) effect, still remains as an important mechanism of nanoparticle accumulation in solid tumors, which is considered to be both a landmark principle in tumor-targeting chemotherapy and an increasingly promising paradigm for anticancer drug development (Fang et al., 2011; Maeda et al., 2009; Torchilin, 2011). Considering the EPR effect and the functionalization process as tools employed to improve tumor accumulation, several papers have been published showing inorganic nanoparticles acting as drug and gene delivery systems.

* Corresponding author. Tel.: +55 31 3069 3223; fax: +55 31 3069 3223.
E-mail address: dcfs@cdtn.br (D.C.F. Soares).

0378-5173/$ – see front matter © 2011 Elsevier B.V. All rights reserved.
doi:10.1016/j.ijpharm.2011.12.002

Among these systems, silica nanoparticles and carbon nanotubes offer promising results (Deng et al., 2011; Slowing et al., 2008). Following the same objectives, recent works have presented boron nitride nanotubes (BNNTs) as new and safe drug delivery systems (Ciofani, 2010; Ciofani et al., 2009). These nanotubes are a structural analog of a carbon nanotube where C atoms are substituted by alternating B and N atoms in a resonance hybrid that shows high structural stability; anti-oxidative ability; as well as chemical, electrical, and mechanical properties that are better than carbon nanotubes (Golberg et al., 2007).

Considering the fact that *in vivo* studies with boron nitride nanotubes have yet to be conducted and based on the context of the EPR effect and the improvement of dispersivity in an aqueous medium, in the present work, these nanotubes were synthesized from a special and facile synthesis route with remarkable yield developed in our laboratory and functionalized using a glycol chitosan polymer according to procedures conducted by Ciofani et al. (2008). After, both physicochemical and morphological characterizations were performed. In addition, *ex vivo* biodistribution and scintigraphic imaging studies, after IV injection, were carried out in an attempt to evaluate their potential as drugs or radioisotope nanocarriers to be applied in therapeutic procedures.

2. Experimental

2.1. Materials

Amorphous boron powder, ammonium nitrate, hematite, and glycol chitosan (MW = 2.5×10^5 Da, degree of deacetylation = 88%) were obtained from Sigma–Aldrich (São-Paulo-Brazil). All solvents used in this study were of analytical grade. All other chemicals used in this study were available commercially at a reagent grade and were used without further purification. MilliQ® water (simplicity 185, Millipore, Bedford, USA) was used throughout the study. All animal experimental protocols were approved by the Ethics Committee for Animal Experiments (CETEA) from the Federal University of Minas Gerais under the code 237/11 and comply with the requirements of the guide for care and use of laboratory animals recommended by the Institute of Laboratory Animal Resources.

2.2. Methods

2.2.1. BNNTs preparation and functionalization

BNNTs samples were prepared based in methods described by Tang et al., 2001 (Tang et al., 2001) with modifications. The powders of NH_4NO_3 (95%, w/w), amorphous boron (97%, w/w), and hematite (95%, w/w and particle size less than 50 nm) were mixed at a molar ratio of 15:15:1, respectively, placed in tubular furnace and heated to 550 °C using an alumina boat as a support. This temperature was kept constant for 1 h. After, the temperature was raised to 1300 °C under a nitrogen gas flow. These conditions were maintained for 1 h. Next, the gas nitrogen flow was interrupted and an ammonia gas flow (50 $cm^3\ s^{-1}$) was added, with samples treated for one additional hour. After having completed these steps, the BNNTs were cooled and successfully obtained with a high yield.

The BNNTs were functionalized (noncovalent coating) with a glycol chitosan polymer, based on the methods described by Ciofani et al. (2010). In a round-bottom flask, 10 mg of BNNTs and 20 mg of glycol chitosan were solubilized in 20 mL of ethanol (99% w/w) and stirred at 70 °C, under reflux for 24 h. After the centrifugation process (10,000 rpm for 10 min), the nanostructures were dispersed in water, where an aqueous dispersion with a concentration of 0.1 mg/mL was obtained. The samples were sonicated for 15 min (Cole Parmer sonicator 750) using an output energy of 10,000 J, resulting in a stable dispersion of BNNTs functionalized with glycol chitosan.

2.2.2. BNNTs physicochemical characterization

2.2.2.1. Scanning electron microscopy (SEM). The morphological characteristics of functionalized BNNTs were studied using the SEM technique. The procedure was performed in a scanning electron microscope (JEOL JSM, 840A) operating at 15 kV. Samples (10 μL) were deposited, spread on silicon substrate and dried with an argon stream. The images were obtained in electron secondary mode, where a minimum of 10 images from each sample was analyzed to assure reproducible results.

2.2.2.2. Thermogravimetry analysis (TGA). Aimed at evaluating the presence of any glycol chitosan polymer under the surface of the BNNTs and its percentage, TGA measurements were taken by a Shimadzu TGA 50WS at a temperature ranging from 25 to 1000 °C. Approximately 3.0 mg of a started mixture and a final sample were analyzed using a heating rate of 10 °C min^{-1}, with a Helium (He) atmosphere flow of 20 mL min^{-1} and an open alumina cell.

2.2.2.3. Fourier transform infrared spectroscopy (FTIR). The FTIR measurements were conducted to complement the results obtained from thermal analysis experiments. The procedure was conducted in a PerkinElmer 1760-X spectrophotometer in the range from 4000 to 400 cm^{-1} with 64 scans and 4 cm^{-1} of resolution.

2.2.2.4. Photon correlation spectroscopy (PCS) and zeta potential analysis. This analytical procedure allows one to determine the mean length of the nanotubes and the polydispersity index (PDI), which is a dimensionless measure of the broadness of the particle size distribution. The analytical procedure was conducted in a Zetasizer Nanoseries Zs (Malvern Instruments, Malvern, UK) apparatus after its adequate dilution in ultra-pure MilliQ® water. The results are expressed as mean ± standard deviation for at least three different batches of each nanotube preparation. The zeta potential was determined by Laser Doppler Anemometry (LDA) in the same Zetasizer equipment. The samples of nanotubes were analyzed following a dilution of 1/1000 in 1 mM of NaCl at a conductivity of approximately 120 ± 20 S/cm^2. The results are reported as the mean ± standard deviation of at least three different batches of each liposome formulation.

2.2.3. BNNTs labeling procedure

The BNNTs were radiolabeled according to the following procedure: 1 mL of BNNTs aqueous solution (1 mg/mL), 10 μL of $SnCl_2$ solution in HCl (1 mg/mL), and 10 μL of $NaHB_4$ solution in NaOH (5 mg/mL) were added to a penicillin flask. The pH was adjusted to 3, 4, 6, 7, 8, 9, 10, and 11, using either NaOH (0.1 N) or HCl (0.1 N) depending on the experiment. Afterwards, a vacuum was made in the flask, and a solution of $Na^{99m}TcO_4$ (37MBq) was added to the mixture. The final solution was stirred at 97 °C for 30 min. The radiolabeling yield of ^{99m}Tc-BNTTs was determined by means of instant thin layer chromatography (ITLC) in two solvent systems: methylethylketone (MEK) to determine TcO_4^- and saline to determine TcO_2.

2.2.4. Biodistribution studies

Biodistribution studies were conducted using two different protocols: (1) *ex vivo* biodistribution study and (2) scintigraphic imaging study and subsequent sacrifice. The studies were conducted based on glycol-chitosan BNNTs radiolabeled with ^{99m}Tc with a radiochemical purity of more than 98%.

2.2.4.1. Ex vivo biodistribution study. Samples of ^{99m}Tc-BNNTs (40 mg/kg) were injected intravenously into the tail of Swiss mice. After periods of 10 and 30 min, and one and 24 h, each animal (three per group) was anesthetized intraperitoneally with a mixture of ketamine and xylazine at a dose of 40 mg/kg and 5 mg/kg, respectively. The blood was collected immediately by cardiac puncture, and the mice were sacrificed by cervical dislocation. The lungs, bladder, intestine, spleen, liver, and kidneys were collected, washed with distilled water, dried on filter paper, and weighed. The determination of radioactivity present in the organs was achieved through automatic scintillation (2470 WIZARD2 Automatic Gamma Counter). The readings were conducted within the 130–150 keV energy window for 10 min. The radioactivity contained in each organ was divided by its mass to furnish the radioactivity in counts per minute per gram of tissue (cpm/g). To set the radioactive decay of ^{99m}Tc, a separate tube with the standard dose containing the same activity and volume of the dose injected into animals was defined as 100% of radioactivity. The %ID/g ratio of tissue was obtained from the relationship between the radioactivity measured in tissue and the radioactivity measured in the standard. The data were statistically analyzed by means of analysis of variance (ANOVA) using a PRISM 5.0 software.

2.2.4.2. Scintigraphic imaging biodistribution study. For the scintigraphic imaging study, BNTTs samples were prepared and radiolabeled to obtain enough activity to acquire the images. The animals were anesthetized intraperitoneally with a ketamine and xylazine solution at a dose of 40 mg/kg and 5 mg/kg, respectively, and were then placed on the table in a supine position so that the detector could be positioned on the anterior region of the animal. The images were obtained with a gamma camera with a collimator-type LEPH 128 × 128 × 32 arrays and an acquisition time of 10 min. Twelve animals were used and all images were obtained from the animals 10 and 30 min; 1, 4 and 24 h after the administration of 11 MBq (40 mg/kg) of radiolabeled BNNTs.

3. Statistical analysis

All experiments were performed in triplicate and expressed as mean ± standard deviation, unless otherwise stated. Mean size and zeta potential data within each time period were compared by means of the ANOVA test, using the software prism 5.0 and considering a probability of 5% as significant.

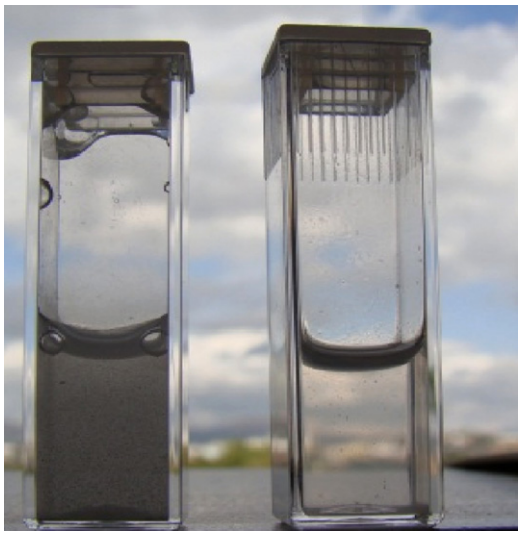

Fig. 1. Samples of BNNTs added in an aqueous solution. On the left cuvette, the BNNT dispersion was not submitted to the functionalization process. On the right cuvette, the BNNTs were functionalized with a glycol chitosan polymer. The presence of the polymer on BNNTs significantly improved the dispersivity of the system.

4. Results and discussion

4.1. BNNTs physicochemical characterization

Fig. 1 shows two different cuvettes where BNNTs samples were added to a volume of 500 μL of water. On the left cuvette, the non-functionalized BNNTs can be observed in a gross dispersion. Here it becomes possible to verify the lower dispersivity of nanostructures in an aqueous solution, forming particle aggregates that are visible to the naked eye, with a strong tendency to deposit on the bottom of flask. The cuvette on the right presents samples of BNNTs functionalized with a glycol chitosan polymer. The polymer coating significantly improved the dispersity of the nanostructures, thus enabling *in vivo* applications.

4.1.1. Scanning electron microscopy

Fig. 2a shows an image of pure BNNTs obtained in our laboratory, whose dimensions are approximately 10 μm in length and 70 nm in diameter. Notably, these are commonly entangled together. Fig. 2b shows that the glycol chitosan that coats the BNNT dispersions

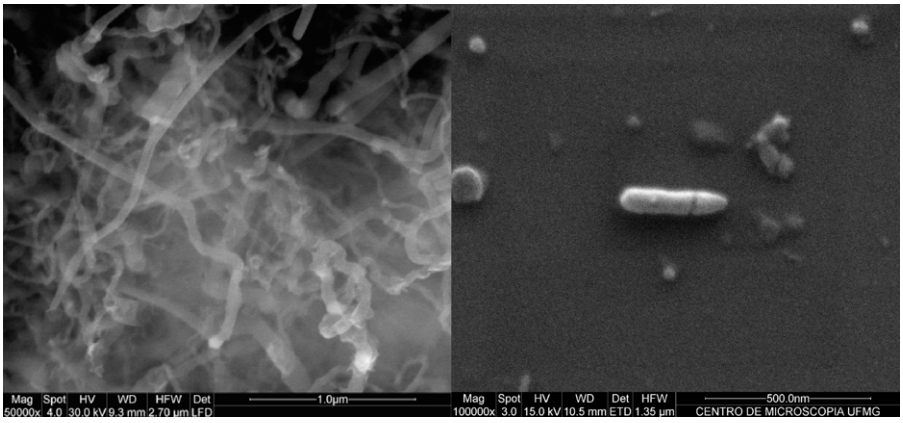

Fig. 2. SEM images of BNNTs before (a) and after the functionalization process (b).

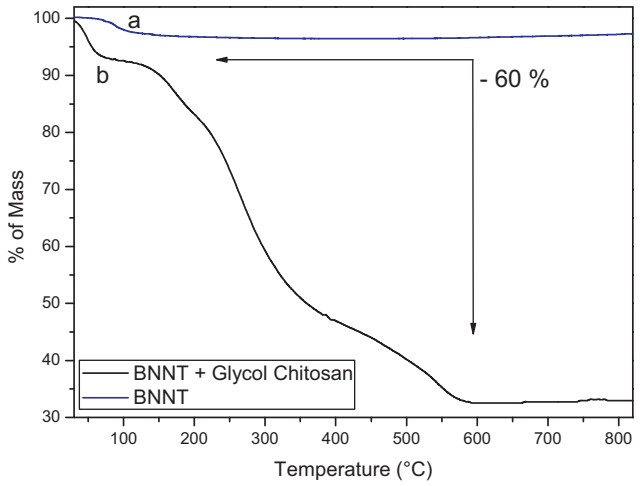

Fig. 3. Thermogravimetric curves of BNNTs before (a) and after (b) the functionalization process.

resulted in remarkably stable and well-dispersed pieces of approximately 300 nm in length and 90 nm in diameter. This considerable increase in the BNNT diameter indicates the efficiency of the functionalization process.

4.1.2. Thermogravimetry analysis

The amount of polymer grafted in the BNNT host was determined by thermogravimetry analysis. The weight loss of the hybrid was evaluated within the range of 25–800 °C. The TGA curves of both samples, pure (a) and functionalized (b), are shown in Fig. 3. Significant weight loss can be observed in the temperature range between 180 °C and 550 °C, corresponding to 60% of the respective initial masses. This finding may be associated with the degradation of the chitosan glycol chains attached to the BNNTs samples.

4.1.3. Fourier transform infrared spectroscopy

Fig. 4 shows the FTIR spectra of glycol chitosan, as well as pure and functionalized BNNT samples. Peak assignments of glycol chitosan (a) are as follows: 3427 cm^{-1} (O—H stretch overlapped with N—H stretch), 2926 cm^{-1} (C—H stretch), 1650 cm^{-1} (amide I band, C=O stretch of acetyl group), 1420–1380 cm^{-1} (C—H bend), 1066 cm^{-1} (C—O stretch) (Yu et al., 2008). In Fig. 4b, the BNNT sample exhibits a strong asymmetric band centered at 1380 cm^{-1}, which corresponds to the bond B—N stretch, along with a less

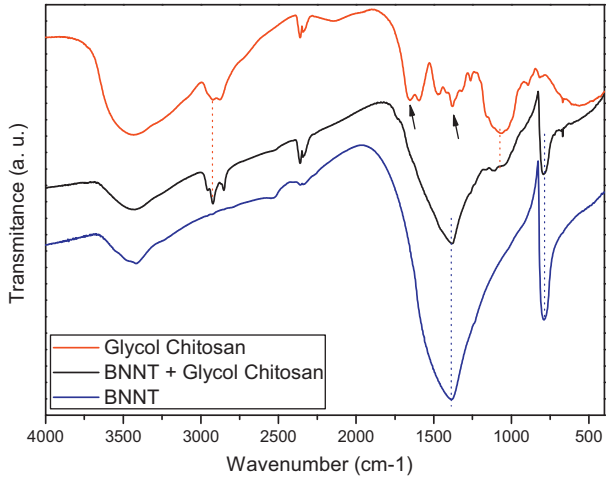

Fig. 4. Infrared spectrum of glycol chitosan (a), BNNT (b), and BNNT + glycol chitosan (c).

Table 1
Physicochemical characteristics of the functionalized BNTTs.

Mean size ± SD (nm) (PCS)[a]	Polydispersity index[b]	ζ Potential ± SD (mV)[c]
290 ± 11	0.18 ± 0.04	−12.4 ± 3.43

[a] Standard deviation (n = 3) of the population that was reported by the instrument.
[b] Monodispersed samples (≤0.3).
[c] Measurement after 1:1000 dilution in 1 mM NaCl (conductivity, 120 ± 20 S/cm).

intense band at 790 cm^{-1} attributed to B—N—B bond (Zheng et al., 2008). It can be observed that some characteristic stretching and bending vibrations present in the glycol chitosan, such as 2926, 2860, and 1370 cm^{-1}, are observed in the functionalized FTIR spectrum sample in Fig. 4c. These results prove the presence of glycol chitosan in the BNNT matrix and demonstrate the successful functionalized procedure used.

4.1.4. Photon correlation spectroscopy and zeta potential analysis

The photon correlation spectroscopy was conducted on 3 samples at different times. The results were calculated from three independent samples by software provided by the manufacturer, which revealed a nearly constant length of nanotubes at 290 nm (Table 1). The PDI found in this study is presented in Table 1. All samples presented a PDI of below 0.3. These results indicate that the process used in nanotube preparation and functionalization allows one to obtain a monodispersed system (<0.3) (de Assis et al., 2008;). The zeta potential of nanotubes can predict its fate *in vivo*, given that the presence of electrical charges minimizes agglomeration and fusion phenomena (Casals et al., 2003). The zeta potential from the formulation exhibited a negative charge, with values of −12 ± 3.7 mV (Table 1).

The zeta potential in cell biology has commonly been used to study many processes in cells, such as activation, agglutination, and adhesion. A study conducted by Cook and Jacobson (1968) showed significant differences in surface electrokinetic properties between normal and cancer cells. Recently, Zhang et al. (2008) reported a significant reduction in the zeta potential values between normal breast epithelial cells and cancer breast epithelial cells (MCF7). The significant differences in the change in surface charges indicate the latent role of zeta potential as a valuable biological signature in studying the cellular interaction of nanoparticles, as well as specific cell functionality. Nanostructures containing significantly positive or negative zeta potential suffer fewer aggregations and merge among themselves, due to the appearance of electrostatic repulsion. Furthermore, the superficial charge of nanostructures has proven to be an important pharmacokinetics regulatory property. For example, studies show that cationic or anionic liposomes activate the complement system through classic or alternative pathway, respectively, leading to a blood serum protein opsonization and subsequent phagocytosis by SMF cells (Chonn et al., 1991).

4.2. BNNTs labeling procedure

Following the described procedure, the BNNTs were radiolabeled in different pHs. Kean and Thanou (2010) observed that chitosan nanoparticles were adsorbed onto the colloidal tin oxides formed by stannous chloride used in the radiolabeling procedure. As such, the authors opted to use sodium borohydride together with stannous chloride to prevent the formation of colloidal particles. According to the authors, this method improved the kinetics of the nanoparticles, resulting in both less blood clearance and liver accumulation. The results show that in acid or alkaline the radiolabel yield decreases significantly when compared to that obtained in neutral pH in which the yield value was greater than 98%, as described in Fig. 5.

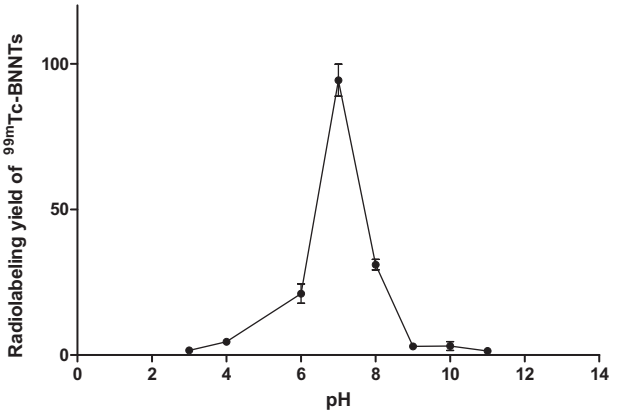

Fig. 5. The influence of pH on the radiolabeling yield of ^{99m}Tc-BNNTs.

4.3. Biodistribution studies

4.3.1. Ex vivo biodistribution study

The investigation of the destination *in vivo (mice)* of BNNTs functionalized with a glycol chitosan polymer was conducted in this study to evaluate the capabilities of this new nanostructure system as a potential carrier system for drugs and radioisotopes for therapeutic purposes. When considering the biodistribution of functionalized BNNTs with glycol chitosan, one must pay attention to the fact that their destination *in vivo* more greatly depends on the polymer coating characteristics than on the bulk of base material and other factors, including shape, size, PDI, and zeta potential. The *ex vivo* biodistribution study is shown in Fig. 6. The results show that, after 30 min, the nanostructures reached systemic circulation and were captured mainly in the liver, spleen, and intestinal tissues, in addition to a significant accumulation in the bladder. This behavior was also observed at times of 1 and 4 h after injection, reflecting an important excretion behavior. It is known that nanostructured systems are taken up by cells of the MPS, which are widely present in the liver, spleen, although the formulations have a hydrophilic polymer of glycol-chitosan coating the nanotubes. These results are consistent with data published by Hyung Park et al. (2006) in a previous study performed with glycol chitosan nanoparticles.

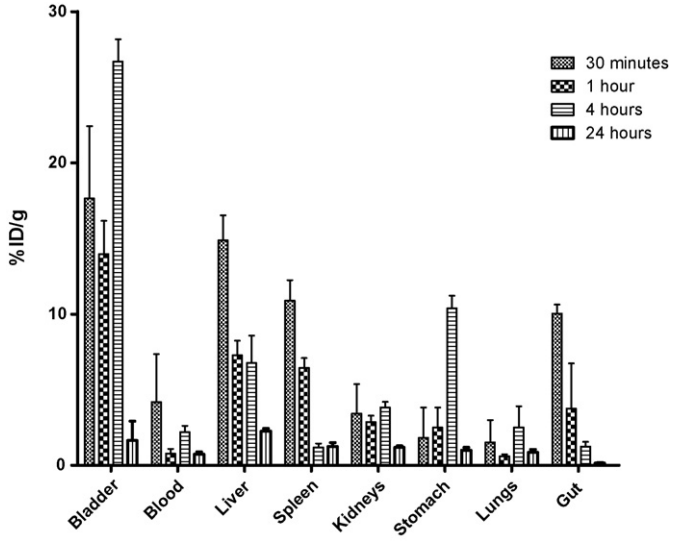

Fig. 6. Biodistribution profile in different tissues at the times: 30 min, 1, 4 and 24 h of glycol chitosan BNNTs. Values expressed as mean ± SD.

The brain and heart were also investigated. However, the radioactivity encountered in these tissues is close to background radiation demonstrating that BNNTs were accumulated in these tissues (data no presented).

One hour after injection, it could be observed that only a small portion of the injected dose remained in the blood tissue (0.79% ID/g), which therefore accumulated in different organs and animal tissues. This result reveals that, in spite of the very hydrophilic character of the glycol chitosan coating, it does not provide the system with a long circulation time, as can be observed in nanostructures, such as "stealth liposomes", where the circulation time is significantly extended by coating the nanostructure with a polymer that is also very hydrophilic, such as PEG (Immordino et al., 2006). This behavior can be explained by the fact that the nanostructures have been extensively excreted by urine and significantly captured by liver and spleen tissues, thus demonstrating the process of identification and phagocytosis by MPS cells. These results are consistent with data published by Banerjee et al. (2002), where glycol chitosan nanoparticles were accumulated, to a great extent, in the liver and spleen tissue. In the same study, the authors also found that, within 6 h after injection, glycol chitosan nanostructures undergo an increasing accumulation in the stomach. In this present study, the equal behavior was observed within 4 h post-injection, contributing to the understanding that glycol chitosan coating significantly impacts the BNNTs destination target *in vivo*.

After 24 h, a low percentage of the injected dose could be observed in all studied organs. This conduct can be explained in part by the high rate of elimination through renal excretion observed and in part by the fact that chitosan and its derivates can be degraded by enzymes such as glucosamine–N-acetyl-glucosamine, hydrolysis glucosamine–glucosamine and N-acetyl-glucosamine–N-acetyl-glucosamine (Kean and Thanou, 2009). Glycol chitosan is thought to be predominantly degraded in vertebrates by lysozymes. In humans, eight chitinases (in the glycoside hydrolase, family 18) have been identified, three of which have shown enzymatic activity (Funkhouser and Aronson, 2007; Zhang and Neau, 2002).

The BNNTs are inorganic nanostructures that cannot be metabolized in the human body. Thus, the most plausible explanation for their clearance from the liver, spleen, and intestines is related to a possible metabolic action performed exclusively with a glycol chitosan coating over the nanostructure as a whole, in turn contributing to the bioaccumulation of non-functionalized BNNTs in these organs.

In previously work, our research group conducted an *in vitro* cytotoxicity study of BNNTs against normal human cells (MRC5 cells – secondary human lung fibroblasts) and murine tumor cells lineages (Ferreira et al., 2011). The results demonstrated that BNNTs do not induce significant cytotoxicity and oxidative stress after 48 h incubation, confirming the optimal biocompatibility and positive evaluation of the biosafety of these nanotubes observed by Ciofani (Ciofani et al., 2010). However, more detailed studies regarding the bioaccumulation of BNNTs in the liver, spleen, intestines, kidneys, and bladder is warranted to better clarify the adverse effects arising from such an accumulation.

4.3.2. Scintigraphic imaging biodistribution study

The scintigraphic imaging biodistribution studies are shown in Fig. 7. The results are compatible with those encountered in the *ex vivo* study. Fig. 7a shows the *in vivo* profile of BNNTs after 30 min (post-tail injection), where the nanostructures are rapidly accumulated in the liver, spleen, and gut tissues. In addition, an important dose could be identified in the kidneys and bladder due to the elimination process. After 1 h and 4 h, in Fig. 7b and c, respectively, a slight clearance from all organs, except the bladder, as well as an accumulation due to the excretion process, can be observed,

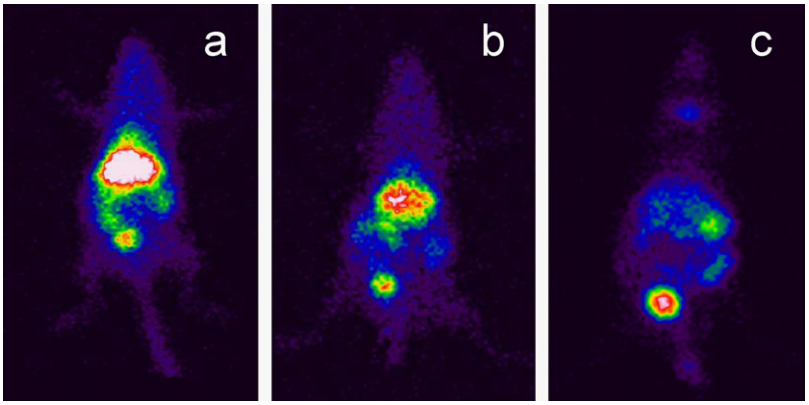

Fig. 7. Scintigraphic image obtained after IV administration of radiolabeled glycol chitosan BNNTs. (a), (b), (c) represents respectively 30 min, 1 and 4 h after injection.

which is in accordance with the *ex vivo* study. After 24 h, the radiation in animals reached a low level that prevented the acquisition of images in a gamma camera. The injected radiation dose would therefore allow for the images to be obtained with relative quality. However, under intense elimination through the kidneys, the total radiation in mice proved to be below the minimum required for image acquisition.

Considering the results encountered in *ex vivo* biodistribution study and scintigraphic imaging, the BNNTs showed *in vivo* behavior similar to that demonstrated by others nanostructured systems like as polymeric micelles and gold nanoparticles showing significant renal elimination and capture by MPS cells (De Jong et al., 2008; Koide et al., 2008). The BNNTs, with mean size of 290 ± 11 nm, exhibit a behavior different from that observed *in vivo* by large nanotubes (>1000 nm) where there is commonly the process of agglomeration and retention in different tissues such as lungs and heart, causing inflammatory responses (Qu et al., 2009). The association of specific molecules, antibodies or aptamers on the surface of BNNTs may allow this system to delivery selectively therapeutic agents in pathological tissues through interaction with specific receptors located in its cells surfaces.

5. Conclusion

The findings in this study revealed that BNNTs were successfully synthesized using a new methodology and functionalized with glycol chitosan. The methodology enabled these nanostructures to have characteristics suitable for *in vivo* distribution studies, where the results revealed a significant elimination of nanostructures by renal excretion and accumulation in the liver, spleen, and intestines. The results showed that, 24 h after the injection, a massive reduction of radiation in the organs where the nanostructures had previously accumulated, in part by intense renal excretion and partly due to a possible metabolism of a glycol chitosan polymer coating with a consequent bioaccumulation of BNNTs in the studied organs. The present results, together with further studies, may reveal a potential application of functionalized BNNTs as new potential drugs or radioisotope nanocarriers to be applied in therapeutic procedures.

Acknowledgments

The authors wish to thank FAPEMIG (Fundação de Amparo a Pesquisa do Estado de Minas Gerais), CNPQ (Conselho Nacional de Desenvolvimento Científico e Tecnológico), and CAPES (Comissão Aperfeiçoamento de Pessoal de Nível Superior) for their financial support.

References

Banerjee, T., Mitra, S., Kumar Singh, A., Kumar Sharma, R., Maitra, A., 2002. Preparation, characterization and biodistribution of ultrafine chitosan nanoparticles. Int. J. Pharm. 243, 93–105.
Casals, E., Galán, A.M., Escolar, G., Gallardo, M., Estelrich, J., 2003. Physical stability of liposomes bearing hemostatic activity. Chem. Phys. Lipids 125, 139–146.
Chonn, A., Cullis, P.R., Devine, D.V., 1991. The role of surface charge in the activation of the classical and alternative pathways of complement by liposomes. J. Immunol. 146, 4234–4241.
Ciofani, G., 2010. Potential applications of boron nitride nanotubes as drug delivery systems. Expert Opin. Drug Deliv. 7, 889–893.
Ciofani, G., Danti, S., D'Alessandro, D., Moscato, S., Menciassi, A., 2010. Assessing cytotoxicity of boron nitride nanotubes: interference with the MTT assay. Biochem. Biophys. Res. Commun. 394, 405–411.
Ciofani, G., Raffa, V., Menciassi, A., Cuschieri, A., 2008. Cytocompatibility, interactions, and uptake of polyethyleneimine-coated boron nitride nanotubes by living cells: confirmation of their potential for biomedical applications. Biotechnol. Bioeng. 101, 850–858.
Ciofani, G., Raffa, V., Menciassi, A., Cuschieri, A., 2009. Folate functionalized boron nitride nanotubes and their selective uptake by glioblastoma multiforme cells: implications for their use as boron carriers in clinical boron neutron capture therapy. Nanoscale Res. Lett. 4, 113–121.
Cook, G.M., Jacobson, W., 1968. The electrophoretic mobility of normal and leukaemic cells of mice. Biochem. J. 107, 549–557.
de Assis, D.N., Mosqueira, V.C.F., Vilela, J.M.C., Andrade, M.S., Cardoso, V.N., 2008. Release profiles and morphological characterization by atomic force microscopy and photon correlation spectroscopy of 99mTechnetium-fluconazole nanocapsules. Int. J. Pharm. 349, 152–160.
de Barros, A.L.B., Mota, L.d.G., Ferreira, C.d.A., Oliveira, M.C.d., Góes, A.M.d., Cardoso, V.N., 2010. Bombesin derivative radiolabeled with technetium-99m as agent for tumor identification. Bioorg. Med. Chem. Lett. 20, 6182–6184.
De Jong, W.H., Hagens, W.I., Krystek, P., Burger, M.C., Sips, A.J.A.M., Geertsma, R.E., 2008. Particle size-dependent organ distribution of gold nanoparticles after intravenous administration. Biomaterials 29, 1912–1919.
Deng, Z., Zhen, Z., Hu, X., Wu, S., Xu, Z., Chu, P.K., 2011. Hollow chitosan-silica nanospheres as pH-sensitive targeted delivery carriers in breast cancer therapy. Biomaterials 32, 4976–4986.
Fang, J., Nakamura, H., Maeda, H., 2011. The EPR effect: unique features of tumor blood vessels for drug delivery, factors involved, and limitations and augmentation of the effect. Adv. Drug Deliv. Rev. 63, 136–151.
Ferreira, T.H., Silva, P.R.O., Santos, R.G., Sousa, E.M.B., 2011. A novel synthesis route do produce boron nitride nanotubes for bioaplications. J. Biomater. Nanobiotechnol. 2, 426–434.
Funkhouser, J.D., Aronson Jr., N.N., 2007. Chitinase family GH18: evolutionary insights from the genomic history of a diverse protein family. BMC Evol. Biol. 7, 1–16.
Golberg, D., Bando, Y., Tang, C.C., Zhi, C.Y., 2007. Boron nitride nanotubes. Adv. Mater. 19, 2413–2432.
Guo, J., Zhang, X., Li, Q., Li, W., 2007. Biodistribution of functionalized multiwall carbon nanotubes in mice. Nucl. Med. Biol. 34, 579–583.
Hocine, O., Gary-Bobo, M., Brevet, D., Maynadier, M., Fontanel, S., Raehm, L., Richeter, S., Loock, B., Couleaud, P., Frochot, C., Charnay, C., Derrien, G., Smaïhi, M., Sahmoune, A., Morère, A., Maillard, P., Garcia, M., Durand, J.-O., 2010. Silicalites and mesoporous silica nanoparticles for photodynamic therapy. Int. J. Pharm. 402, 221–230.
Huynh, N.T., Passirani, C., Saulnier, P., Benoit, J.P., 2009. Lipid nanocapsules: A new platform for nanomedicine. Int. J. Pharm. 379, 201–209.
Hyung Park, J., Kwon, S., Lee, M., Chung, H., Kim, J.-H., Kim, Y.-S., Park, R.-W., Kim, I.-S., Bong Seo, S., Kwon, I.C., Young Jeong, S., 2006. Self-assembled nanoparticles based on glycol chitosan bearing hydrophobic moieties as carriers for

doxorubicin: in vivo biodistribution and anti-tumor activity. Biomaterials 27, 119–126.
Immordino, M.L., Dosio, F., Cattel, L., 2006. Stealth liposomes: review of the basic science, rationale, and clinical applications, existing and potential. Int. J. Nanomed. 1, 297–315.
Kean, T., Thanou, M., 2009. Chitin and chitosan—sources, production and medical applications. In: Williams, P., Arshady, R. (Eds.), Desk Reference of Natural Polymers, their Sources, Chemistry and Applications. Kentus Books, London, pp. 327–361.
Kean, T., Thanou, M., 2010. Biodegradation, biodistribution and toxicity of chitosan. Adv. Drug Deliv. Rev. 62, 3–11.
Klumpp, C., Kostarelos, K., Prato, M., Bianco, A., 2006. Functionalized carbon nanotubes as emerging nanovectors for the delivery of therapeutics. Biochim. Biophys. Acta Biomembr. 1758, 404–412.
Koide, H., Asai, T., Hatanaka, K., Urakami, T., Ishii, T., Kenjo, E., Nishihara, M., Yokoyama, M., Ishida, T., Kiwada, H., Oku, N., 2008. Particle size-dependent triggering of accelerated blood clearance phenomenon. Int. J. Pharm. 362, 197–200.
Maeda, H., Bharate, G.Y., Daruwalla, J., 2009. Polymeric drugs for efficient tumor-targeted drug delivery based on EPR-effect. Eur. J. Pharm. Biopharm. 71, 409–419.
Qu, G., Bai, Y., Zhang, Y., Jia, Q., Zhang, W., Yan, B., 2009. The effect of multiwalled carbon nanotube agglomeration on their accumulation in and damage to organs in mice. Carbon 47, 2060–2069.
Sakamoto, J.H., van de Ven, A.L., Godin, B., Blanco, E., Serda, R.E., Grattoni, A., Ziemys, A., Bouamrani, A., Hu, T., Ranganathan, S.I., De Rosa, E., Martinez, J.O., Smid, C.A., Buchanan, R.M., Lee, S.-Y., Srinivasan, S., Landry, M., Meyn, A., Tasciotti, E., Liu, X., Decuzzi, P., Ferrari, M., 2010. Enabling individualized therapy through nanotechnology. Pharmacol. Res. 62, 57–89.
Slowing, I.I., Vivero-Escoto, J.L., Wu, C.-W., Lin, V.S.Y., 2008. Mesoporous silica nanoparticles as controlled release drug delivery and gene transfection carriers. Adv. Drug Deliv. Rev. 60, 1278–1288.
Soares, D.C.F., de Oliveira, M.C., de Barros, A.L.B., Cardoso, V.N., Ramaldes, G.A., 2011. Liposomes radiolabeled with 159Gd: in vitro antitumoral activity, biodistribution study and scintigraphic image in Ehrlich tumor bearing mice. Eur. J. Pharm. Sci. 43, 290–296.
Safi, M., Courtois, J., Seigneuret, M., Conjeaud, H., Berret, J.F., 2011. The effects of aggregation and protein corona on the cellular internalization of iron oxide nanoparticles. Biomaterials 32, 9353–9363.
Tang, C.C., Fan, S.S., Li, P., Liu, Y.M., Dang, H.Y., 2001. Synthesis of boron nitride in tubular form. Mater. Lett. 51, 315–319.
Torchilin, V., 2011. Tumor delivery of macromolecular drugs based on the EPR effect. Adv. Drug Deliv. Rev. 63, 131–135.
Vauthier, C., Persson, B., Lindner, P., Cabane, B., 2011. Protein adsorption and complement activation for di-block copolymer nanoparticles. Biomaterials 32, 1646–1656.
Xiong, L.-Q., Chen, Z.-G., Yu, M.-X., Li, F.-Y., Liu, C., Huang, C.-H., 2009. Synthesis, characterization, and in vivo targeted imaging of amine-functionalized rare-earth up-converting nanophosphors. Biomaterials 30, 5592–5600.
Yu, J.-M., Li, Y.-J., Qiu, L.-Y., Jin, Y., 2008. Self-aggregated nanoparticles of cholesterol-modified glycol chitosan conjugate: preparation, characterization, and preliminary assessment as a new drug delivery carrier. Eur. Polym. J. 44, 555–565.
Zhang, H., Neau, S.H., 2002. In vitro degradation of chitosan by bacterial enzymes from rat cecal and colonic contents. Biomaterials 23, 2761–2766.
Zhang, Y., Yang, M., Portney, N.G., Cui, D., Budak, G., Ozbay, E., Ozkan, M., Ozkan, C.S., 2008. Zeta potential: a surface electrical characteristic to probe the interaction of nanoparticles with normal and cancer human breast epithelial cells. Biomed. Microdevices 10, 321–328.
Zheng, M., Liu, Y., Gu, Y., Xu, Z., 2008. Synthesis and characterization of boron nitride sponges as a novel support for metal nanoparticles. Sci. China Chem. 51, 205–210.